AIAA JOURNAL
Vol. 35, No. 1, January 1997

Large Eddy Simulation of an Equilibrium Three-Dimensional Turbulent Boundary Layer

Xiaohua Wu* and Kyle D. Squires†
University of Vermont, Burlington, Vermont 05405

Large eddy simulation has been applied to prediction of an equilibrium three-dimensional turbulent boundary layer (TBL). Subgrid-scale stresses were parameterized using a Lagrangian dynamic mixed model. The predicted mean velocities and second-order statistics are in good agreement with direct numerical simulation results. Single-point statistics are also generally similar to those found in other equilibrium three-dimensional TBLs such as the flow over a rotating disk and the turbulent Ekman layer. The modification of shear stress producing structure by mean flow three-dimensionality was also investigated. Joint probability density functions show that in the buffer region the contribution to the shear stress from strong ejections is slightly larger than that from strong sweeps. The conditionally averaged velocity fluctuations in the buffer region indicate that streamwise vortices of the same sign as the near-wall mean streamwise vorticity produce strong sweeps but weakened ejections, whereas those with the opposite sign produce strong ejections but weakened sweeps. These features are found to persist within a moderate increase in the Reynolds number, corresponding to a 20% reduction in the peak mean crossflow velocity, and are consistent with similar measures obtained in the turbulent flow over a rotating disk.

I. Introduction

A THREE-DIMENSIONAL turbulent boundary layer (TBL) is a complex wall-bounded flow in which the direction of the mean velocity varies continuously with distance from the wall; examples include the boundary layer over a swept wing and the flow over a rotating disk. One of the most well-known features of three-dimensional TBLs is that the vector formed by the turbulent stress parallel to the wall is not aligned with the mean strain rate (e.g., Refs. 1–3). Accurate simulation and modeling remain difficult due to this and other complicating features. For example, because of the misalignment between stress and strain, predictions obtained using isotropic eddy viscosity models will be inaccurate and ad hoc modification of the eddy viscosity to account for the misalignment will yield a coordinate-dependent model applicable to only a narrow class of flows.[4] Thus, more versatile predictive approaches are required.

Large eddy simulation (LES) offers a promising technique for simulation of complex flows such as three-dimensional TBLs. In considering prediction of three-dimensional TBLs it is important to distinguish between equilibrium and nonequilibrium flows. Equilibrium boundary layers exhibit relatively slow streamwise variation and the mean velocity may be collapsed by an appropriate scaling while analogous scalings for nonequilibrium boundary layers do not exist (e.g., Ref. 5). Experimental measurements have been obtained mostly in nonequilibrium three-dimensional TBLs in which a crossflow is induced by imposition of a spanwise pressure gradient on an initially two-dimensional boundary layer (e.g., Refs. 4 and 6–10). Because of the complex configurations considered in the experiments, measurements tend to be sensitive to geometry and details of the upstream conditions. For instance, three-dimensional TBLs can become considerably more complex when the spanwise pressure gradient reverses sign (due to a streamwise variation of geometry), with the possibility of a complete reversal in sign of the mean crossflow in the inner part with respect to that in the outer part of the boundary layer (e.g., Ref. 11).

Direct numerical simulation (DNS) has also been a useful tool for exploring nonequilibrium three-dimensional TBLs. Moin et al.,[12] Senstad and Moin,[13] and Coleman et al.[14] applied a spanwise pressure gradient to a fully developed turbulent channel flow. Consistent with experiments in nonequilibrium three-dimensional TBLs, the simulations show a reduction in the Reynolds shear stress as well as in the turbulence kinetic energy with increasing transverse strain. The directions of the Reynolds shear stress vector and the mean velocity gradient vector were also found to differ. Sendstad and Moin[13] found that Reynolds stress production is suppressed by streamwise vortices of both signs (with respect to the near-wall mean streamwise vorticity) as compared with a two-dimensional boundary layer. Recent findings reported by Coleman et al.[14] are in agreement with the earlier work of Sendstad and Moin.[13] The DNS database obtained by Coleman et al.[14] was also used by Piomelli et al.[15] in a priori tests of subgrid-scale (SGS) models for large eddy simulation. Piomelli et al.[15] found that, in general, nonequilibrium effects on the subgrid scales appear to be less significant than on the large scales.

Equilibrium three-dimensional TBLs are produced over infinite geometries and are three-dimensional from inception. Experimental measurements have been obtained in the flow over a rotating disk (e.g., Ref. 2 and references therein) as well as through DNS of the turbulent Ekman layer[3] and the three-dimensional TBL created by a rotating freestream velocity vector.[1] Spalart[1] and Coleman et al.[3] presented detailed boundary-layer statistics, showing that the directions of the Reynolds shear stress vector parallel to the wall alternately lead/lag that of the mean strain rate across the layer. The mean velocity obeys the law of the wall but lacks an obvious wake component. A reduction in the stress/energy ratio, common to nonequilibrium three-dimensional TBLs, was also observed. For the purpose of evaluating LES predictions, an advantage of considering equilibrium boundary layers is that they are relatively free from effects of system parameters, e.g., geometry and initial conditions. Thus, the focus of this study is the equilibrium boundary layer created by a rotating freestream velocity vector computed by Spalart[1] using DNS. The flow is one of the simplest that can produce mean flow three-dimensionality, is statistically homogeneous in planes parallel to the wall, and evolves to an equilibrium independent of its initial conditions.

The principal improvement in development of LES as a viable means for prediction of complex turbulent flows has been dynamic SGS modeling. In dynamic formulations, model coefficients are calculated using the resolved (large-scale) field rather than specified a priori. Several studies have demonstrated that dynamic models work well in a wide variety of flows, yielding satisfactory results when compared with experiments or DNS results (e.g., Refs. 16–24). Application of LES and dynamic models to three-dimensional TBLs

Received March 14, 1996; revision received April 30, 1996; accepted for publication Sept. 13, 1996; also published in *AIAA Journal on Disc*, Volume 2, Number 1.

*Postdoctoral Associate, Department of Mechanical Engineering.
†Assistant Professor, Department of Mechanical Engineering.

is needed to further advance the technique as a tool for prediction of complex turbulent flows.

There are two main issues that must be addressed in applying LES and dynamic models to prediction of three-dimensional TBLs. The first is the particular parameterization of the SGS stress. In most applications, SGS stresses have been modeled using eddy viscosity formulations in which the SGS stress is assumed to be aligned with the resolved strain rate. Zang et al.[18] relaxed this constraint by formulating a dynamic mixed model in their computation of a driven cavity flow. Vreman et al.[22] later discussed a mathematical inconsistency associated with the Zang et al.'s model and obtained improved predictions of a temporally evolving mixing layer using a mathematically consistent mixed model. Since the turbulent stress and mean strain are not aligned in three-dimensional TBLs, a mixed model is an appropriate choice for parameterization of SGS stresses in three-dimensional TBLs.

The second issue relevant to application of dynamic models to three-dimensional TBLs is determination of the model coefficient C. One of the main advantages of the dynamic formulation is that it yields a coefficient that can, in principal, be evaluated on a point-by-point basis. However, in practice averages over homogeneous directions have been employed in the majority of previous work to avoid ill-conditioning associated with a local determination of C (e.g., Ref. 19). Various investigators have developed localized versions in which averaging is performed only over small regions in space[18,24] or along particle trajectories.[21] Ghosal et al.[23] employed a variational formulation to determine the model coefficient as a function of space and time, obtaining accurate predictions of isotropic turbulence and the flow over a backward-facing step. The computational overhead associated with the variational formulation, however, can be significant. The Lagrangian formulation developed by Meneveau et al.[21] yielded accurate predictions of canonical flows such as isotropic turbulence as well as transitional and fully developed channel flow, with a relatively minor increase in simulation overhead. Since spatial averaging is not required in the Lagrangian approach formulated by Meneveau et al.,[21] it is an attractive candidate for use in complex flows. Thus, the primary objective of this study is application of LES to prediction of three-dimensional TBLs using the dynamic mixed model proposed by Vreman et al.[22] in which the model coefficient is determined using the Lagrangian formulation of Meneveau et al.[21]

Though the flow created by a rotating freestream is geometrically simple, the three-dimensional TBL that results is complex and also resembles in many respects the disk flow of Littell and Eaton.[2] Littell and Eaton[2] found that the location of the peak crossflow velocity did not scale with inner variables, though outer-layer scaling was not indicated since the boundary-layer thickness was difficult to measure because of the very low velocities at the boundary-layer edge. Littell and Eaton[2] also concluded that the underlying structure of three-dimensional TBLs is similar to that advanced by Robinson[25] but with modifications caused by the presence of the spanwise mean flow. A secondary interest of this work is to examine the structure of the three-dimensional TBL created by a rotating freestream velocity and, in particular, to examine whether structural features similar to those measured by Littell and Eaton[2] exist.

An overview of the simulations is presented in the following section. As shown in Sec. II, a Lagrangian dynamic mixed model is formulated that uses the Lagrangian approach developed by Meneveau et al.[21] for computation of the model coefficient. LES predictions are compared with the DNS results of Spalart[1] in Sec. III.A. Structural measures obtained using conditional sampling are presented in Sec. III.B in the context of their similarities and differences to similar measures obtained in the disk flow of Littell and Eaton.[2]

II. Simulation Overview

The boundary layer is created over a stationary infinite plate by a rotating freestream velocity as shown in Fig. 1. The pressure gradient together with the no-slip condition imposed on the plate produces a skewed spanwise velocity profile. The flow is homogeneous in planes parallel to the wall and therefore prescription of inflow/outflow boundary conditions is not needed. As shown in the figure, the freestream velocity has a magnitude U_0 and rotates at frequency f, which yields velocities in the x–z laboratory system $u_\infty = U_0 \cos(ft)$ and $w_\infty = U_0 \sin(ft)$. The associated pressure gradient is

$$\frac{\partial p}{\partial x}_\infty = fU_0 \sin(ft) \qquad \text{and} \qquad \frac{\partial p}{\partial z}_\infty = -fU_0 \cos(ft)$$

The velocity vector rotates in planes parallel to the wall, and therefore the wall-normal axis y is unaffected by the rotating freestream. On planes parallel to the wall, following Spalart,[1] a total of four sets of coordinate axes are used and are shown schematically in Fig. 1: x–z axes denote the stationary inertial laboratory system; x'–z' axes refer to a coordinate system aligned with freestream where the freestream velocity vector is directed along the positive x' axis; and x''–z'' axes are aligned with the wall shear stress vector, where the resultant wall shear stress Π_w is in the positive x'' direction, making an angle α with the freestream velocity vector. The final set of x'''–z''' axes was introduced by Spalart[1] to account for the misalignment between the wall shear stress vector and Reynolds shear stress vector in a three-dimensional TBL. The angle between x''' and x'' is $\phi^* = \alpha - C_5(\nu f)/u_\tau^2$, where u_τ is the friction velocity.[1] The constant C_5 is defined as the integral of the velocity deviation from the log law in the viscous sublayer. Spalart[1] obtained $C_5 = 52$ using flat-plate data from two-dimensional boundary layers.

Having defined the various coordinate systems, the same superscript as used to define the coordinate axes shall be used to refer to quantities projected in that system. Fluctuating quantities shall be denoted using a t subscript. For instance, $\overline{u}_t$ is the grid-filtered instantaneous fluctuating velocity component along the x' axis obtained via $\overline{u}_t = \overline{u}' - \langle \overline{u}' \rangle$, where $\langle\ \rangle$ represents an average over time and homogeneous directions. The $+$ superscript represents normalization by the friction velocity u_τ. Vector and second-order tensor transformations among the four systems are performed using standard tensor algebra operations.

Mass and momentum conservation is enforced for the large-scale resolved variables, which are obtained by filtering the Navier–Stokes equations:

$$\frac{\partial \bar{u}_j}{\partial x_j} = 0 \tag{1}$$

$$\frac{\partial \bar{u}_i}{\partial t} + \frac{\partial}{\partial x_j}\bar{u}_i\bar{u}_j = -\frac{\partial \bar{p}}{\partial x_i} - \frac{\partial}{\partial x_j}\tau_{ij} + \frac{1}{Re_l}\frac{\partial^2 \bar{u}_i}{\partial x_j^2} \tag{2}$$

In Eqs. (1) and (2) an overbar denotes the filtered variable. Velocities are normalized by the freestream value U_0, lengths by the viscous depth $\delta_l = \sqrt{(2\nu/f)}$, where ν is the kinematic viscosity. The Reynolds number is then $Re_l = U_0\delta_l/\nu$.

Following Germano,[26] the SGS stress τ_{ij} in Eq. (2) is written as

$$\tau_{ij} = \mathcal{L}_{ij} + \mathcal{C}_{ij} + \mathcal{R}_{ij} \tag{3}$$

where $\mathcal{L}_{ij}$, $\mathcal{C}_{ij}$, and $\mathcal{R}_{ij}$ are the modified Leonard, cross, and SGS Reynolds stresses, respectively. As discussed in the previous section, it is well known that the turbulent shear stress is not aligned

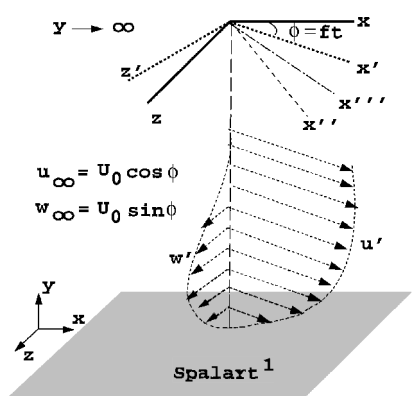

Fig. 1 Schematic of the three-dimensional TBL created over a stationary infinite plate by a rotating freestream velocity.

with the mean strain rate in three-dimensional TBLs. In the context of LES, although the anisotropy of the SGS motions is expected to be smaller than that of the large scales, the alignment forced between SGS stress and resolved-scale strain in eddy viscosity parameterizations of Eq. (3) is troublesome. Inaccuracies associated with forced alignment between stress and strain can be overcome by explicitly calculating the modified Leonard stress $\mathcal{L}_{ij}$ and using an eddy viscosity model for the cross term and SGS Reynolds stress. This approach has been used by Zang et al.[18] and Vreman et al.[22] in the formulation of dynamic mixed models, and τ_{ij} can be expressed as

$$\tau_{ij} - (\delta_{ij}/3)\tau_{kk} = -2C\bar{\Delta}^2|\bar{S}|\bar{S}_{ij} + \mathcal{L}_{ij} - (\delta_{ij}/3)\mathcal{L}_{kk} \quad (4)$$

(see also Ref. 27) In Eq. (4), δ_{ij} is the Kronecker delta, $\bar{\Delta} = (\bar{\Delta}_x\bar{\Delta}_y\bar{\Delta}_z)^{1/3}$, and $|\bar{S}| = \sqrt{(2\bar{S}_{ij}\bar{S}_{ij})}$ is the magnitude of the large-scale strain rate tensor $\bar{S}_{ij} = (\partial\bar{u}_i/\partial x_j + \partial\bar{u}_j/\partial x_i)/2$. The modified Leonard stress is $\mathcal{L}_{ij} = \overline{u_i u_j} - \bar{u}_i\bar{u}_j$ and, as shown by Germano,[26] guarantees Galilean invariance.

In both Zang et al.[18] and Vreman et al.[22] spatial averaging was used to determine the model coefficient C. In this work C is determined using the Lagrangian approach developed by Meneveau et al.[21] in which averaging is performed along fluid pathlines rather than over directions of statistical homogeneity. The principal advantage of the Lagrangian formulation is that the coefficient can be determined on a point-by-point basis and also contains history information. Thus, the formulation of the dynamic mixed model is identical to that proposed by Vreman et al.[22] but with a model coefficient C determined using the Lagrangian approach of Meneveau et al.[21]

Following Meneveau et al.,[21] the model constant can be expressed as the ratio of two integrals, i.e., $C(\mathbf{x}, t) = I_{LM}/I_{MM}$, where I_{LM} and I_{MM} are solutions to separate transport equations. To reduce the computational cost associated with evaluation of I_{LM} and I_{MM}, Meneveau et al.[21] adopted a simple time discretization. A similar approach is adopted in this work in which the evolution of I_{LM} and I_{MM} for the closure (4) can be expressed as

$$\frac{I_{LM}^{n+1}(\mathbf{x}) - I_{LM}^{n}(\mathbf{x} - \bar{\mathbf{u}}\Delta t)}{\Delta t} = \frac{1}{T^n}\left\{[(L_{ij} - H_{ij})M_{ij}]^{n+1}(\mathbf{x}) - I_{LM}^{n+1}(\mathbf{x})\right\} \quad (5)$$

$$\frac{I_{MM}^{n+1}(\mathbf{x}) - I_{MM}^{n}(\mathbf{x} - \bar{\mathbf{u}}\Delta t)}{\Delta t} = \frac{1}{T^n}\left\{[M_{ij}M_{ij}]^{n+1}(\mathbf{x}) - I_{MM}^{n+1}(\mathbf{x})\right\} \quad (6)$$

where $T = 2\bar{\Delta}I_{LM}^{-1/4}$ is the time scale characterizing the exponential memory,

$$L_{ij} = \widehat{\bar{u}_i\bar{u}_j} - \hat{\bar{u}}_i\hat{\bar{u}}_j, \qquad M_{ij} = -2(\hat{\bar{\Delta}}^2|\hat{\bar{S}}|\hat{\bar{S}}_{ij} - \bar{\Delta}^2\widehat{|\bar{S}|\bar{S}_{ij}})$$

and

$$H_{ij} = \widehat{\hat{\bar{u}}_i\hat{\bar{u}}_j} - \hat{\bar{u}}_i\hat{\bar{u}}_j - (\widehat{\overline{u_iu_j}} - \widehat{\bar{u}_i\bar{u}_j}) \quad (7)$$

Note that test filtering required for dynamic evaluation of the model coefficient is denoted using $\hat{\ }$. Multiple filtering operations are performed sequentially.[18,22]

The quantities I_{LM}^{n} and I_{MM}^{n} denote values at the previous time step and are obtained by linear interpolation. The new values I_{LM}^{n+1} and I_{MM}^{n+1} on the grid are then obtained. The result is a weighted sum of the interpolated prior value and the current source term on the grid:

$$I_{LM}^{n+1}(\mathbf{x}) = H\left\{\epsilon[(L_{ij} - H_{ij})M_{ij}]^{n+1}(\mathbf{x}) + (1-\epsilon)I_{LM}^{n}(\mathbf{x} - \bar{\mathbf{u}}\Delta t)\right\} \quad (8)$$

$$I_{MM}^{n+1}(\mathbf{x}) = \epsilon[M_{ij}M_{ij}]^{n+1}(\mathbf{x}) + (1-\epsilon)I_{MM}^{n}(\mathbf{x} - \bar{\mathbf{u}}\Delta t) \quad (9)$$

where

$$\epsilon = \frac{\Delta t/T^n}{1 + \Delta t/T^n} \qquad \text{and} \qquad H(\chi) = \begin{cases} \chi & \text{if } x \geq 0 \\ 0 & \text{otherwise} \end{cases} \quad (10)$$

The ramp function H is introduced to clip the solution away from complex values.

The governing equations (1) and (2) were solved using the fractional step method.[28] Second-order central differences were used for approximation of spatial derivatives together with a mixed explicit/implicit time advancement of the discretized equations. The continuity constraint was enforced by solving the Poisson equation for pressure using fast transforms together with tridiagonal matrix inversion. At the upper boundary of the computational domain, the velocity was specified as $\bar{u} = U_0\cos(ft)$, $\bar{v} = 0$, and $\bar{w} = U_0\sin(ft)$. No-slip boundary conditions were used at the wall $y = 0$, and periodic boundary conditions were incorporated in the x and z directions.

Calculations were performed at $Re_l = 7.67\times10^2$ and 9.53×10^2. As will be shown in Sec. III, this change in Reynolds number results in a 20% reduction in the degree of mean-flow skewing. In Spalart[1] the Reynolds number was varied from 5.00×10^2 to 7.67×10^2 and in the Ekman layer simulations of Coleman et al.[3] from 4×10^2 to 5×10^2. The size of the computational domain is guided by the DNS of Spalart[1] and Coleman et al.[3] The horizontal dimensions L_x and L_z are 1.6δ, where $\delta = u_\tau/f$ is the turbulent boundary-layer thickness (compared with 1.8δ used by Coleman et al.[3]). In terms of the viscous depth, L_x and L_z are $34.4\delta_l$ at $Re_l = 7.67\times10^2$ and $40.64\delta_l$ at $Re_l = 9.53\times10^2$. Spalart[1] found that increasing the horizontal dimensions from 2δ to 4δ increased the friction velocity u_τ by only 0.5%. Coleman et al.[3] found that the change in two-point correlation functions by a similar increase in L_x and L_z is minimal. The height of the computational box also extends to 1.6δ.

The initial Cartesian velocity was prescribed as the laminar solution superimposed with random fluctuations. From the initial instant, the governing equations for the large-scale field were integrated using a coarse grid (33^3). After a statistically steady state had been achieved (around 10 inertial time periods), the velocity fields from the coarse grid computation were interpolated to a 65^3 grid. The resolution in wall units was $\Delta x^+ = \Delta z^+ = 23$ at $Re_l = 7.67\times10^2$ and 32 at $Re_l = 9.53\times10^2$. Integration was then continued to convergence. The sample size was taken to be one inertial period $T = 2\pi/f$, similar to that used by Coleman et al.[3] For the 65^3 LES, the total number of grid points is about 5% of that used in the DNS by Spalart[1] at $Re_l = 7.67\times10^2$. Use of the Lagrangian dynamic mixed model increases the computational cost of the calculation by about 70% compared with simulations performed using the dynamic eddy viscosity model of Germano et al.[16] in which averaging over homogeneous planes is required to ensure numerical stability. CPU requirements for calculations using the dynamic eddy viscosity model with plane averaging are about 20% greater than in simulations with no SGS model. Though the simulation cost is increased due to the use of the Lagrangian mixed model, the overall cost of the LES remains substantially smaller than a DNS.

III. Results

A. Statistical Measures

Mean velocity profiles at $Re_l = 7.67\times10^2$ are compared with the DNS results of Spalart[1] in Fig. 2a. Overall, there is good agreement between LES predictions obtained using the Lagrangian dynamic mixed model and DNS data with a slight overprediction of the streamwise velocity. LES predictions of the friction velocity u_τ and wall shear stress angle α are within 2 and 1%, respectively, of the DNS results of Spalart.[1] Also shown are LES predictions obtained from the dynamic eddy viscosity model of Germano et al.[16] in which averages over x–z planes are used for evaluation of the model coefficient. A larger overshoot in both the mean streamwise and spanwise velocities is apparent using the eddy viscosity formulation. As a result of the system transformation shown in Fig. 1, the spanwise component $\langle\overline{w'''}\rangle$ is negative above $y^+ = 10$. The streamwise component obeys the familiar log law within $30 < y^+ < 200$, indicating a similarity of the three-dimensional TBL to canonical two-dimensional boundary layers (see also Ref. 1). However, there is no obvious wake component in the distribution of $\langle\overline{u'''}\rangle^+$. Figure 2b shows the mean velocity polar plot for both Reynolds numbers. Consistent with Spalart[1] and Coleman et al.,[3] the profile becomes more shallow with increasing Reynolds number and is significantly different from the laminar solution. At $Re_l = 7.67\times10^2$ and 9.53×10^2, the maximum spanwise velocity $\langle\overline{w'}\rangle_p$ is $0.19U_0$ and $0.15U_0$, respectively, a 20% decrease in $\langle\overline{w'}\rangle_p$ corresponding to a reduction in the degree of

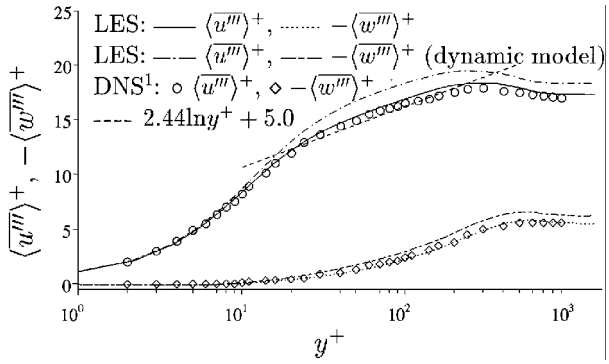

a) Comparison with Spalart[1] at $Re_l = 7.67 \times 10^2$

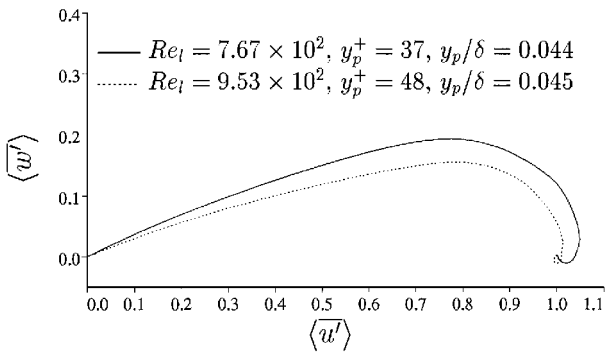

b) Polar plot

Fig. 2 Mean velocity distributions.

mean-flow skewing. Figure 2b also shows that, within the Reynolds number range considered, the height y_p of the peak spanwise velocity appears to scale with outer coordinates ($y_p/\delta \approx 0.044$), consistent with recent work in three-dimensional TBLs summarized by Eaton.[29] In terms of inner coordinates, $y_p^+ = 37$ for $Re_l = 7.67 \times 10^2$ and 48 for $Re_l = 9.53 \times 10^2$.

Turbulence intensities and resolved shear stresses (including the SGS contributions) are compared with the DNS results from Spalart[1] in Fig. 3. As shown in Fig. 3a, in the inner region between $15 < y^+ < 50$, LES predictions of the streamwise component $\overline{u'''}^+_{rms}$ are greater than DNS results, whereas the wall-normal fluctuations $\overline{v}^+_{rms}$ are smaller, a behavior often observed in LES calculations. When plotted in outer coordinates (Fig. 3b), resolved turbulence intensities in the LES show good agreement with Spalart[1] throughout the boundary layer. Reynolds shear stress profiles plotted in inner and outer coordinates are shown in Figs. 3c and 3d, respectively. The two primary shear stresses $-\langle\overline{u'''v}\rangle^+$ and $-\langle\overline{w'''v}\rangle^+$ predicted in the LES are in excellent agreement with the DNS results. The other off-diagonal stress, $\langle\overline{u'''w'''}\rangle$, although not zero, does not contribute to the transport of mean momentum. Also apparent is the sharp reduction in $-\langle\overline{u'''v}\rangle$ relative to profiles typically observed in canonical two-dimensional boundary layers. Similar behavior in the $-\langle\overline{u'''v}\rangle$ stress is also evident in DNS calculations and experiments of other equilibrium three-dimensional TBLs (e.g., Refs. 2 and 3). This reduction is principally due to the action of the favorable spanwise pressure gradient $\partial p_\infty/\partial z = -fU_0$ (Refs. 30 and 31).

Characteristics of the SGS model are shown in Fig. 4. Figure 4a shows the contribution to the SGS stress from the eddy viscosity part of the model, $2\langle C\Delta^2|\bar{S}|\bar{S}_{ij}\rangle'''^+$, as well as that from the modified Leonard stress components $\overline{\mathcal{L}}_{ij}$. The signs of the stresses follow the resolved stresses shown in Fig. 3. The magnitude of the modified Leonard stresses is generally larger than the corresponding modeled stress components. This is consistent with the channel

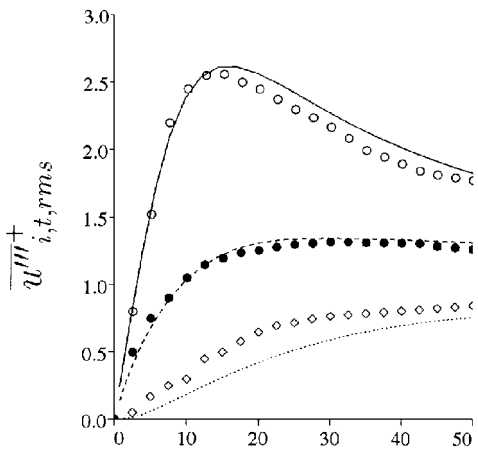

a) Intensities

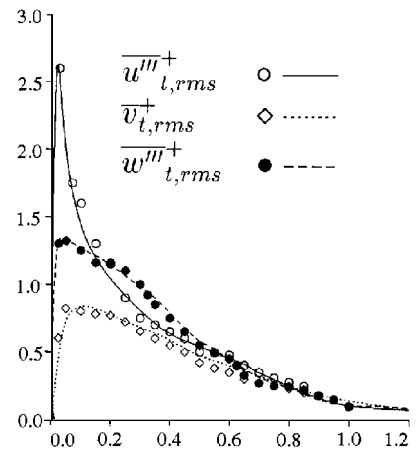

b) Intensities

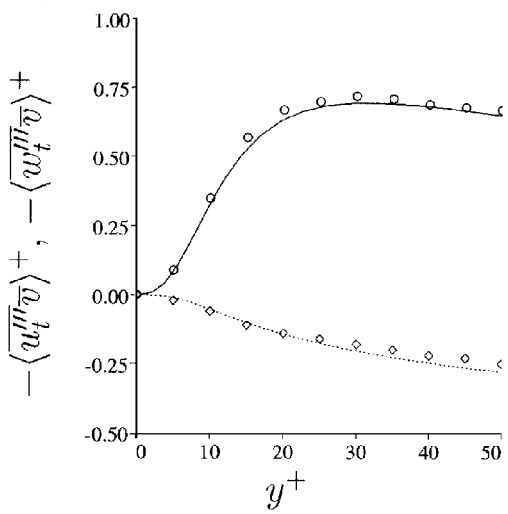

c) Shear stresses

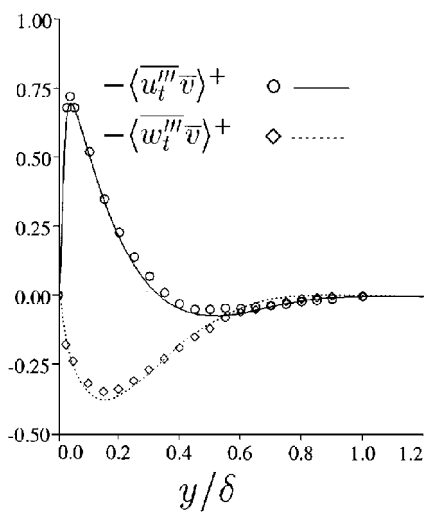

d) Shear stresses

Fig. 3 Turbulence intensities and resolved shear stresses, $Re_l = 7.67 \times 10^2$; lines, LES; symbols, Spalart.[1]

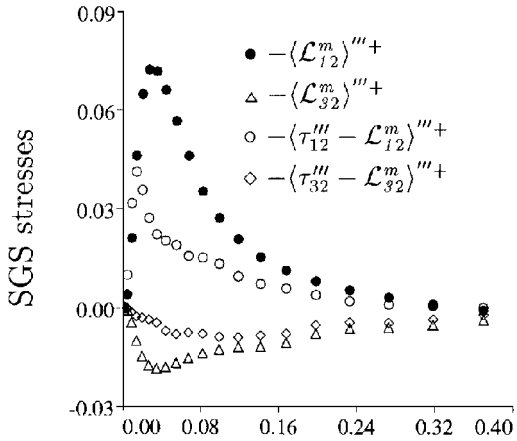

a) Averaged SGS stress components

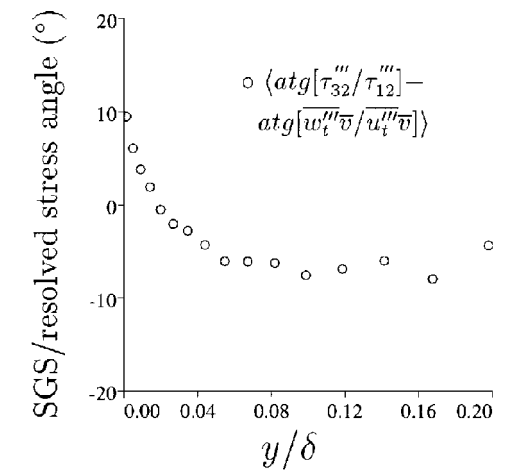

b) Relative angle between SGS stress vector and resolved turbulent shear stress vector

Fig. 4 Model characteristics, $Re_l = 7.67 \times 10^2$.

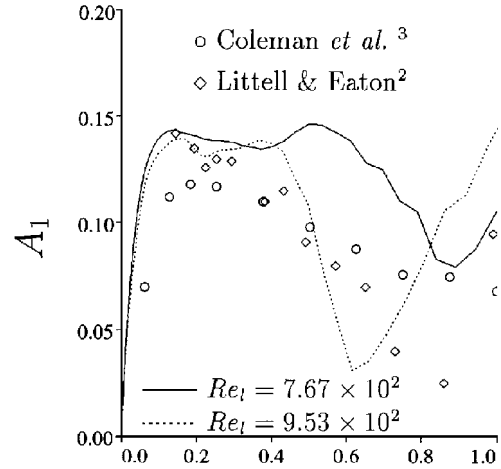

a) A_1

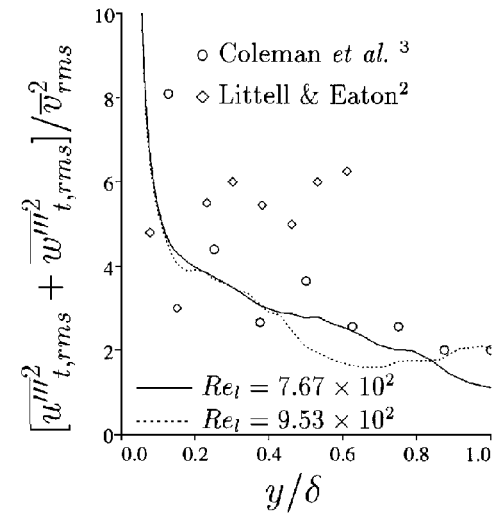

b) $[\overline{u'''_{t,rms}}^2\ \overline{w'''_{t,rms}}^2]/v^2_{rms}$

Fig. 5 Structural parameters.

flow calculations of Cabot[32] in which the dynamic mixed model of Zang et al[18] was employed and $\mathcal{L}_{12}$ was larger than the modeled part throughout the channel. Shown in Fig. 4b is the relative angle between the SGS stress vector and resolved turbulent stress vector. Note the angle is an average of the local angles, which are calculated from the local stresses. Only the results below $y/\delta = 0.2$ are shown since in the outer region the angle depends increasingly on the ratio of small quantities and is unreliable. It may be observed that, on average, below $y/\delta = 0.02$ the SGS stress leads the resolved stress, whereas for $0.02 < y/\delta < 0.2$ the SGS stress vector lags the resolved stresses. Also note that the misalignment between the SGS and resolved stresses is small, with a maximum about 10 deg located at the wall. Though not shown here, the angle formed by the resolved stresses and mean strain rate alternates throughout the layer with a maximum deviation of less than 15 deg below $y/\delta = 0.4$. The lead/lag in the angle throughout the layer is similar to that observed by Spalart[1] and Coleman et al.[3] in DNS of equilibrium three-dimensional TBLs. A relatively small angle between the turbulent shear stress and mean strain was also measured by Littell and Eaton.[2]

One measure of the efficiency of shear stress generation for a given amount of energy is the structural parameter

$$A_1 = \frac{\left[\left\langle \overline{u'''v} \right\rangle^2 + \left\langle \overline{w'''v} \right\rangle^2\right]^{\frac{1}{2}}}{\overline{u'''^2_{rms}} + \overline{v}^2_{rms} + \overline{w'''^2_{rms}}}$$

For a canonical flat-plate boundary layer, A_1 is between 0.15 and 0.16 throughout most of the layer (e.g., Ref. 4). Shown in Fig. 5a are profiles of A_1 at both Reynolds numbers. Included with the profiles are the Ekman layer results from Coleman et al.[3] at $Re_l = 4 \times 10^2$ and the experimental measurements from a rotating disk at $Re_\theta = 1.66 \times 10^3$ from Littell and Eaton.[2] Within $0.1 < y/\delta < 0.4$, A_1 for the current three-dimensional TBL is between 0.13 and 0.14, slightly lower than the values for two-dimensional boundary layers. Above $y/\delta = 0.4$, A_1 decreases as in the Ekman layer and the disk flow, although the values in this region should be viewed with caution due to uncertainties in their calculation. The three flows shown in Fig. 5 are equilibrium three-dimensional TBLs and bear common features such as rotation and infinite geometry. As discussed by Littell and Eaton,[2] the irrotational motions in the outer region dominate these three-dimensional TBLs and cause strong attenuation of A_1. In spatially developing nonequilibrium three-dimensional TBLs such as the one studied by Anderson and Eaton,[6] A_1 was suppressed near the wall and this suppression diffused outward, possibly due to decreased importance of the outer irrotational motion. The ratio of the wall-parallel normal stresses to wall-normal stress is shown in Fig. 5b, together with the results from Coleman et al.[3] and Littell and Eaton.[2] In boundary layers this structural parameter is often used as a crude measure of the efficiency of turbulent mixing (e.g., Ref. 33). The current three-dimensional TBL and Ekman layer show a reduction in this quantity with increasing distance from the wall, indicating an increase in the efficiency of turbulent mixing. The reduction observed in Fig. 5b is also consistent with that observed in nonequilibrium, pressure-driven three-dimensional TBL experiments (e.g., Ref. 6). Littell and Eaton,[2] however, observed an increase in the ratio with increasing distance from the wall and a peak in the outer region of the boundary layer. One factor that could play a role in producing such a difference is the vertical entrainment in the disk flow.

B. Structural Measures

As shown earlier, the statistical measures predicted in the LES are in good agreement with the DNS results of Spalart.[1] Many

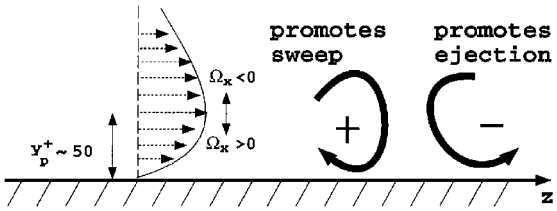

Fig. 6 Three-dimensional TBL structural model advanced by Littell and Eaton[2] and Eaton.[29]

of the trends observed in the LES are also present in the Ekman layer considered by Coleman et al.[3] as well as the equilibrium three-dimensional TBL over a rotating disk studied by Littell and Eaton.[2] Several observations can be made from these and other three-dimensional TBL studies. First, certain differences exist between three-dimensional TBLs and two-dimensional boundary layers and also between equilibrium and nonequilibrium three-dimensional TBLs. Most notably, in a nonequilibrium three-dimensional TBL the direction of the shear stress vector usually lags that of the strain rate, whereas in the present three-dimensional TBL and Ekman layer the vectors lead/lag throughout the layer (in a two-dimensional boundary layer the stress and strain are aligned). Littell and Eaton[2] found a relatively small lag of the shear stress relative to the strain rate. Second, in nonequilibrium three-dimensional TBLs the parameter A_1 usually increases with the distance from the wall, whereas in an equilibrium three-dimensional TBL A_1 decreases in the outer region. Furthermore, A_1 is also lower than the corresponding value in two-dimensional boundary layers.

There are also indications that the structures of attached three-dimensional TBLs are not drastically different from those in two-dimensional boundary layers. For example, the law of the wall applies to the mean streamwise velocity[11]; quasistreamwise vortices and low- and high-speed streaks exist below $y^+ = 100$.[14,29] This suggests that the shear stress producing structure in a three-dimensional TBL is a modification (by the crossflow) of the structure existing in two-dimensional boundary layers. In an effort to understand the modification of shear stress production, Littell and Eaton[2] carried out conditional sampling experiments in the three-dimensional TBL over a rotating disk. Littell and Eaton[2] considered the near-wall coherent structure model of Robinson[25] in a canonical flat-plate boundary layer as an approximation to the shear stress producing structure in a three-dimensional TBL. In Robinson's model most ejections are found on the upstream side of transverse vortices, which often form head elements of one- or two-sided vortical arches; strong sweeps occur primarily on the outboard side of tilted necks. Based on this baseline model and their conditionally sampled velocity field, Littell and Eaton[2] proposed that the modification of shear stress producing structure by mean-flow three-dimensionality is that the crossflow reduces the ability of streamwise vortices of one sign to produce strong ejections, while weakening the ability of those of vortices of the other sign to produce strong sweeps (see also Ref. 29). The sense of rotation of the streamwise vortices with respect to that of the near-wall mean streamwise vorticity is shown in Fig. 6. The model presented by Littell and Eaton[2] and Eaton[29] represents a significant step forward towards an improved understanding of the structural features of three-dimensional TBLs. However, also note that Flack and Johnston[34] found that in a nonequilibrium three-dimensional TBL the modification of the near-wall structure appears different than that advanced by Littell and Eaton.[2] The situation is phrased by Littell and Eaton[2] as follows: "Two-point velocity correlations from other three-dimensional boundary layers, particularly those based on 'infinite' geometries are needed to evaluate coherent structure models as modified by three-dimensionality." Thus, it is of interest in this study to investigate the modification of near-wall shear stress producing structures. In particular, the same structural measures considered in Littell and Eaton[2] are presented in Figs. 7–9.

Contributions of the large eddies to turbulent stresses can be studied by conditionally sampling the joint probability density function

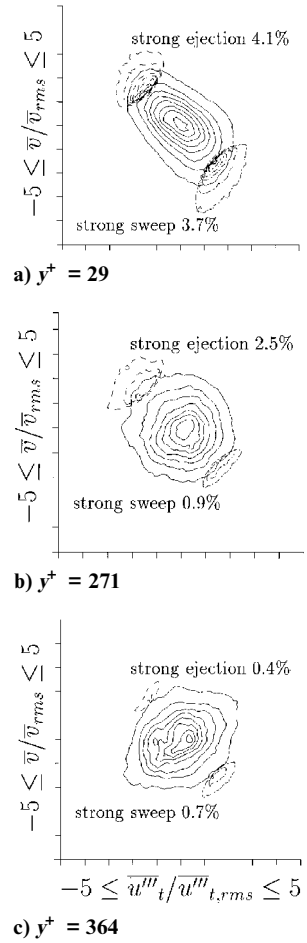

Fig. 7 Joint probability density function $B(\overline{u\psi'}, \overline{v})$ and $Re_l = 7.67 \times 10^2$; note that the origin is at (−5, −5): ——, $B(\overline{u\psi'}, \overline{v})\Delta\overline{u\psi'}\Delta\overline{v}$, increasing from 0.02% towards center in increments of 0.04%; - - -, strong ejections $B_E(\overline{u\psi'}, \overline{v})\Delta\overline{u\psi'}\Delta\overline{v}$, increasing from 0.004% by 0.008%; and – – –, strong sweeps $B_S(\overline{u\psi'}, \overline{v})\Delta\overline{u\psi'}\Delta\overline{v}$, increasing from 0.004% by 0.008%.

of the instantaneous velocity fluctuations. The joint probability density function $B(\overline{u\psi'}, \overline{v})$ is defined as

$$B(\overline{u\psi'}, \overline{v})\Delta\overline{u\psi'}\Delta\overline{v} = \lim_{\mathcal{T}\to\infty} \frac{1}{\mathcal{T}} \sum \Delta\mathcal{T} \quad \Delta\overline{u\psi'} \to 0,\ \Delta\overline{v} \to 0 \tag{11}$$

where $\Delta\mathcal{T}$ is the time the fluctuations spend inside the window $(\overline{u\psi'} \pm \Delta\overline{u\psi'}, \overline{v} \pm \Delta\overline{v})$. The window width was chosen to be one-eighth the corresponding rms fluctuation. The conditional probability for a strong ejection, $B_E(\overline{u\psi'}, \overline{v})$, is calculated by sampling $B(\overline{u\psi'}, \overline{v})$ based on $|\overline{u\psi'}\overline{v}| \ge 2\overline{u\psi'}_{rms}\overline{v}$ and $\overline{v} > 0$. The condition for a strong sweep event, $B_S(\overline{u\psi'}_t, \overline{u\psi'}_t)$, is similarly defined with $\overline{v} < 0$. Shown in Fig. 7 are contours of $B(\overline{u\psi'}, \overline{v})$, $B_E(\overline{u\psi'}, \overline{v})$, and $B_S(\overline{u\psi'}, \overline{v})$ for $Re_l = 7.67 \times 10^2$ at three elevations $y^+ = 29$, 271, and 364 ($y/\delta = 0.035$, 0.32, and 0.45). These locations correspond to $-\langle\overline{u\psi'}\overline{v}\rangle$ obtaining its maximum, zero, and minimum values (see Fig. 3c and 3d). Near the surface, contours of $B(\overline{u\psi'}, \overline{v})$ are tilted toward the II–IV quadrant. Further above this elevation, the degree of tilting decreases gradually and the contours become axisymmetric, corresponding to the zero stress value at the second elevation. Above the second elevation, tilting is toward the I–III quadrant where the sign of the stress $-\langle\overline{u\psi'}\overline{v}\rangle$ changes from positive to negative. In a two-dimensional boundary layer the Reynolds stress generally does not change sign across the layer; except for separated flows (e.g., see Baskaran et al.[35]). Figure 7 also shows the likelihood of strong ejection and strong sweep events. At the elevation near the surface where the stress $-\langle\overline{u\psi'}\overline{v}\rangle$ is maximum, $\sum B_E(\overline{u\psi'}, \overline{v}) \approx 1.1 \sum B_S(\overline{u\psi'}, \overline{v})$, indicating in the buffer region where $-\langle\overline{u\psi'}\overline{v}\rangle$ is large, contributions of strong ejections to this stress component are only slightly larger than strong sweeps. As

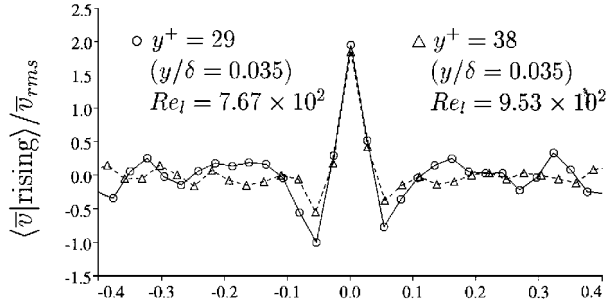

a) Rising event $\bar{v}_{r_3'=0} > 1.4\bar{v}_{rms}$

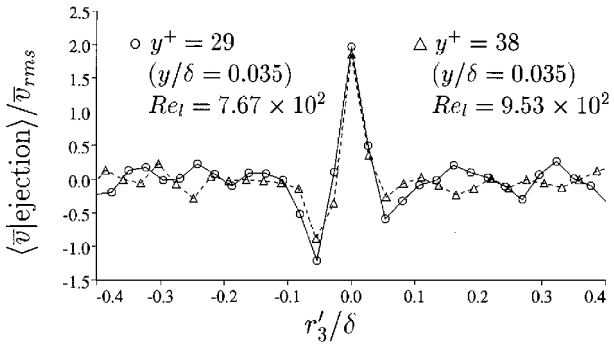

b) Strong ejection event $\overline{u_{l,r_3'=0}\bar{v}_{r_3'=0}} < -2\overline{u_{l,rms}\bar{v}_{rms}}, \bar{v}_{r_3'=0} < 0.$

Fig. 8 Conditionally averaged wall-normal fluctuations at the elevation of maximum $\langle\overline{u_l v}\rangle$.

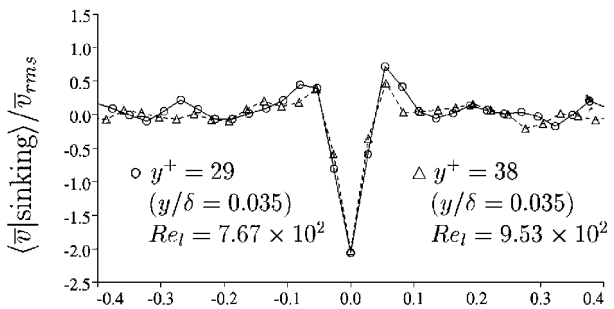

a) Sinking event $\bar{v}_{r_3'=0} < -1.4\bar{v}_{rms}$

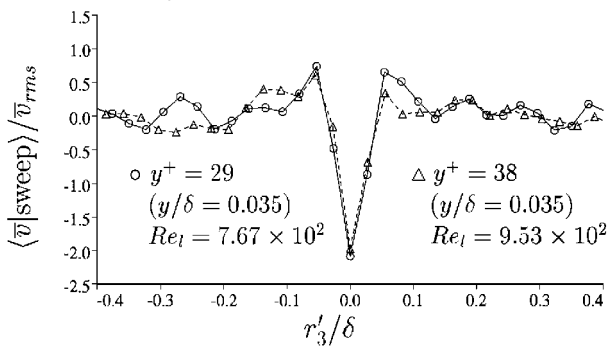

b) Strong sweep event $\overline{u_{l,r_3'=0}\bar{v}_{r_3'=0}} < -2\overline{u_{l,rms}\bar{v}_{rms}}, \bar{v}_{r_3'=0} < 0$

Fig. 9 Conditionally averaged wall-normal fluctuations at the elevation of maximum $\langle\overline{u_\theta v}\rangle$.

discussed in Robinson,[25] in a canonical two-dimensional boundary layer ejection motions are the major contributor to Reynolds shear stress in the region beyond $y^+ \approx 12$. Visualizations by Anderson and Eaton[6] showed that wall streaks in their three-dimensional TBL appeared more stable, suggesting that bursting occurs less frequently in a boundary layer with mean-flow skewing (see also Ref. 29). Flack and Johnston[34] found that three-dimensionality appears to stabilize the near-wall region by producing fewer vortical ejection events, which is also consistent with the smaller ratio of ejections to sweeps shown in Fig. 7a. The results in Fig. 7 are then consistent with the notion that the structure in a three-dimensional TBL is a modification of that in a two-dimensional boundary layer.

In a canonical two-dimensional boundary layer, the contribution to upward and downward motion by streamwise vortices of either sign is statistically the same (see Fig. 6). Although the vortical structure may not necessarily occur side by side, the contribution to strong ejection (or strong sweep) motion by streamwise vortices of either sign is also statistically identical (e.g., Refs. 25 and 36). Thus, further insight into the modification of near-wall turbulence by mean-flow three-dimensionality may be gained by looking into the behavior of conditionally averaged wall-normal fluctuations.

Figure 8a shows the average wall-normal fluctuations near a rising event, defined similarly to Littell and Eaton[2] as $\bar{v}_{r_3'=0} > 1.4\bar{v}_{rms}$. In a canonical two-dimensional boundary layer the distribution is symmetric with respect to the origin. As seen in Fig. 8a, relative to the origin $r_3'/\delta = 0$ the upward vertical motion around a rising event is asymmetric on the upstream and downstream side of the crossflow. However, the degree of asymmetry is small, indicating an approximately equal contribution from positively signed (same as mean streamwise vorticity below y_p, see Fig. 6) and negatively signed streamwise vortices. This quasisymmetry is consistent with the crossflow not destroying streamwise vortices having the opposite sign as the mean streamwise vorticity. Figure 8b shows the average wall-normal velocity near a strong ejection event, $\overline{u_{l,r_3'=0}\bar{v}_{r_3'=0}} < -2\overline{u_{l,rms}\bar{v}_{rms}}, \bar{v}_{r_3'=0} > 0$. The vertical motion in the vicinity of a strong ejection has a larger degree of asymmetry with respect to $r_3' = 0$, which suggests a nonuniform modification by the crossflow of structures producing these events. On average, around a strong ejection the crossflow on the downstream side has a larger upward motion compared with the upstream side. This indicates that strong ejections are more likely to be associated with negatively signed streamwise vortices, as illustrated schematically in the structural model of Littell and Eaton[2] in Fig. 6. Note that if strong ejections are more likely to be associated with positively signed vortices, one would find a larger downward motion on the downstream side of the crossflow, which would be contrary to the results shown in Fig. 8b. Also note that the conditional sampling is carried out in the buffer region where the primary shear stress is maximum (at $y^+ = 29$ and 38 for $Re_l = 7.67 \times 10^2$ and 9.53×10^2, respectively). This elevation is below the location of the peak in the mean crossflow velocity ($y_p^+ = 37$ and 48; see Fig. 2b). Conditionally sampled data from Littell and Eaton[2] at $Re_\theta = 1.66 \times 10^3$ was obtained at $y^+ = 133$, which was above the elevation corresponding to the peak in the mean crossflow velocity ($y_p^+ = 60$ in their work). The results shown in Fig. 8 exhibit very similar features as measured by Littell and Eaton.[2]

Similar observations can be made by studying the average wall-normal fluctuations near sinking events, defined as $\bar{v}_{r_3'=0} < -1.4\bar{v}_{rms}$. As shown in Fig. 9, around a sinking event, the downward vertical motion exhibits only a slight asymmetry with respect to the origin, again indicating the existence of nearly equal numbers of positively and negatively signed streamwise vortices. Shown in Fig. 9b are the average wall-normal fluctuations near a strong sweep event. The asymmetry in the wall-normal fluctuations is not as strong as observed in Fig. 8b but does appear to suggest a nonuniform modification of the structures responsible for strong sweeps. On average, around a strong sweep event, the downstream side of the crossflow has a larger downward motion compared with the upstream side. This indicates that strong sweeps are more likely to be associated with positively signed vortices (cf. Fig. 6). If this were not true, i.e., if strong sweep events are more likely to be associated with negatively signed vortices, one would find a larger upward motion on the downstream side of the crossflow. Although not shown here, certain off-diagonal two-point correlations with nonzero spanwise separation and that are symmetric in a two-dimensional flat-plate boundary layer are strongly asymmetric in the present three-dimensional TBL.[37] The asymmetry in spanwise velocity correlations and the behavior shown in Figs. 7–9 are similar to those measured in the experiment by Littell and Eaton[2] and support the structural model advanced in their work.

IV. Summary

Large eddy simulation of an equilibrium three-dimensional TBL was performed. The flow considered is one of the simplest that can produce mean-flow three-dimensionality; it is statistically homogeneous in planes parallel to the wall and evolves to an equilibrium independent of its initial conditions. A Lagrangian dynamic mixed model was formulated to parameterize the SGS stress. The computed mean velocity components, turbulence intensities, and Reynolds stresses show good agreement with the DNS results.

Single-point statistics are similar to the DNS Ekman layer results and existing measurements from a rotating disk. In these flows the mean streamwise velocity obeys the usual log law, but without an obvious wake component, shear stresses show a significant reduction compared with canonical two-dimensional boundary layers. Unlike other nonequilibrium three-dimensional TBLs, A_1 in these equilibrium three-dimensional TBLs tends to decrease in the outer layer. Joint probability density functions show that in the buffer region the contribution to the turbulent shear stress from strong ejections is slightly higher than that from strong sweeps. Conditionally sampled velocity fluctuations around rising/sinking and around strong ejection/sweep events tend to support Eaton's three-dimensional TBL structural model. In the presence of a crossflow, although the total number of positively and negatively signed streamwise vortices are approximately the same, their ability to produce shear stress is modified by mean-flow three-dimensionality, leaving vortices of one sign that are more efficient at producing ejections, whereas those of the other sign are more efficient at producing sweep. These properties, though possibly not applicable to spatially developing nonequilibrium three-dimensional TBLs, are to some degree universal for equilibrium three-dimensional TBLs, especially those over infinite geometry, which are three dimensional from inception.

Acknowledgments

This work is supported by the Office of Naval Research (Grants N00014-94-1-1053 and N00014-94-1-0047; Program Officer, L. P. Purtell). Computer time for the simulations was supplied by the Cornell Theory Center. Helpful comments on the work from P. Bradshaw, G. Coleman, J. Eaton, and P. Spalart are also gratefully acknowledged.

References

[1]Spalart, P. R., "Theoretical and Numerical Study of a Three-Dimensional Turbulent Boundary Layer," *Journal of Fluid Mechanics*, Vol. 205, Aug. 1989, pp. 319–340.

[2]Littell, H. S., and Eaton, J. K., "Turbulence Characteristics of the Boundary Layer on a Rotating Disk," *Journal of Fluid Mechanics*, Vol. 266, May 1994, pp. 175–207.

[3]Coleman, G. N., Ferziger, J. H., and Spalart, P. R., "A Numerical Study of the Turbulent Ekman Layer," *Journal of Fluid Mechanics*, Vol. 213, April 1990, pp. 313–348.

[4]Bradshaw, P., and Pontikos, N. S., "Measurements in the Turbulent Boundary Layer on an Infinite Swept Wing," *Journal of Fluid Mechanics*, Vol. 159, Oct. 1985, pp. 105–130.

[5]Tennekes, H., and Lumley, L., *A First Course in Turbulence*, 1st ed., MIT Press, Cambridge, MA, 1972, Chap. 5.

[6]Anderson, S. D., and Eaton, J. K., "Reynolds Stress Development in Pressure-Driven Three-Dimensional Turbulent Boundary Layers," *Journal of Fluid Mechanics*, Vol. 202, May 1989, pp. 263–294.

[7]Flack, A. K., and Johnston, J. P., "Near-Wall Investigation of Three-Dimensional Turbulent Boundary Layers," Dept. of Mechanical Engineering, Stanford Univ., Rept. MD-63, Stanford, CA, July 1993.

[8]Ha, S. M., and Simpson, R. L., "An Experimental Investigation of Three-Dimensional Turbulent Boundary Layers Using Multiple-Sensor Probes," *Proceedings of the 9th Symposium Turbulent Shear Flow* (Kyoto, Japan), 1993, pp. 2-3-1–2-3-6.

[9]Schwarz, W. R., and Bradshaw, P., "Turbulence Structural Changes for a Three-Dimensional Turbulent Boundary Layer in a 30° Bend," *Journal of Fluid Mechanics*, Vol. 272, Aug. 1994, pp. 183–209.

[10]Simpson, R. L., and Olcmen, S. M., "An Experimental Study of a Three-Dimensional Pressure-Driven Turbulent Boundary Layer," *Journal of Fluid Mechanics*, Vol. 290, May 1995, pp. 225–262.

[11]Johnston, J. P., and Flack, K. A., "Review: Advances in Three-Dimensional Turbulent Boundary Layers with Emphasis On the Wall-Layer Regions," *Journal of Fluids Engineering*, Vol. 118, June 1996, pp. 219–236.

[12]Moin, P., Shih, T. H., Driver, D., and Mansour, N. N., "Direct Numerical Simulation of a Three-Dimensional Turbulent Boundary Layer," *Physics of Fluids A*, Vol. 2, No. 10, 1990, pp. 1846–1853.

[13]Sendstad, O., and Moin, P., "The Near Wall Mechanics of Three-Dimensional Turbulent Boundary Layers," Dept. of Mechanical Engineering, Stanford Univ., Rept. TF-57, Stanford, CA, Dec. 1992.

[14]Coleman, G. N., Kim, J., and Le, A. T., "A Numerical Study of Three-Dimensional Boundary Layers," *Proceedings of the 10th Symposium Turbulent Shear Flow*, Univ. of Pennsylvania, University Park, PA, 1995, pp. 3-29-7–3-29-12.

[15]Piomelli, U., Coleman, G., and Kim, J., "Effects of Mean Flow Three-Dimensionality on the Subgrid-Scale Stresses," *Bulletin of the American Physical Society*, Vol. 40, No. 12, 1995, p. 1958.

[16]Germano, M., Piomelli, U., Moin, P., and Cabot, W. H., "A Dynamic Subgrid-Scale Eddy Viscosity Model," *Physics of Fluids A*, Vol. 3, No. 7, 1991, pp. 1760–1765.

[17]Moin, P., Squires, K. D., and Cabot, W., "A Dynamic Subgrid-Scale Model for Compressible Turbulence and Scalar Transport," *Physics of Fluids A*, Vol. 3, No. 11, 1991, pp. 2746–2757.

[18]Zang, Y., Street, R. L., and Koseff, J. R., "A Dynamic Mixed Subgrid-Scale Model and Its Application to Turbulent Recirculating Flows," *Physics of Fluids A*, Vol. 5, No. 12, 1993, pp. 3186–3195.

[19]Piomelli, U., "High Reynolds Number Calculations Using the Dynamic Subgrid-Scale Stress Model," *Physics of Fluids A*, Vol. 5, No. 6, 1993, pp. 1484–1490.

[20]Yang, K. S., and Ferziger, J. H., "Large Eddy Simulation of Turbulent Obstacle Flow Using a Dynamic Subgrid-Scale Model," *AIAA Journal*, Vol. 31, No. 8, 1993, pp. 1406–1413.

[21]Meneveau, C., Lund, T. S., and Cabot, W., "A Lagrangian Dynamic Subgrid-Scale Model of Turbulence," *Proceedings of the Summer Program*, Center for Turbulence Research, Stanford Univ., Stanford, CA, 1994, pp. 1–29.

[22]Vreman, B., Geurts, B., and Kuerten, H., "On the Formulation of the Dynamic Mixed Subgrid-Scale Model," *Physics of Fluids*, Vol. 6, No. 12, 1994, pp. 4057–4059.

[23]Ghosal, S., Lund, T. S., Moin, P., and Akselvoll, K., "A Dynamic Localization Model for Large Eddy Simulation of Turbulent Flows," *Journal of Fluid Mechanics*, Vol. 286, March 1995, pp. 229–255.

[24]Piomelli, U., and Liu, J., "Large Eddy Simulation of Rotating Channel Flows Using a Localized Dynamic Model," *Physics of Fluids*, Vol. 7, No. 4, 1995, pp. 839–848.

[25]Robinson, S. K., "Coherent Motions in the Turbulent Boundary Layer," *Annual Review of Fluid Mechanics*, Vol. 23, 1991, pp. 601–639.

[26]Germano, M., "A Proposal for a Redefinition of the Turbulent Stresses in the Filtered Navier–Stokes Equations," *The Physics of Fluids*, Vol. 29, No. 7, 1986, pp. 2323, 2324.

[27]Bardina, J., Ferziger, J. H., and Reynolds, W. C., "Improved Turbulence Models Based on LES of Homogeneous Incompressible Turbulent Flows," Dept. of Mechanical Engineering, Stanford Univ., Rept. TF-19, Stanford, CA, Sept. 1984.

[28]Kim, J., and Moin, P., "Application of a Fractional-Step Method to Incompressible Navier–Stokes Equations," *Journal of Computational Physics*, Vol. 59, No. 2, 1985, pp. 308–323.

[29]Eaton, J. K., "Effects of Mean Flow Three-Dimensionality on Turbulent Boundary-Layer Structure," *AIAA Journal*, Vol. 33, No. 11, 1995, pp. 2020–2025.

[30]Csanady, G. T., "On the Resistance Law of a Turbulent Ekman Layer," *Journal of the Atmospheric Sciences*, Vol. 24, Sept. 1967, pp. 467–471.

[31]Bradshaw, P., private communication, Dept. of Mechanical Engineering, Stanford Univ., Stanford, CA, July 1995.

[32]Cabot, W., "Local Dynamic Subgrid-Scale Models in Channel Flow," *Annual Research Briefs*, Center for Turbulence Research, Stanford Univ., Stanford, CA, 1994, pp. 143–157.

[33]Murlis, J., Tsai, H. M., and Bradshaw, P., "The Structure of Turbulent Boundary Layers at Low Reynolds Numbers," *Journal of Fluid Mechanics*, Vol. 122, Sept. 1982, pp. 13–56.

[34]Flack, A. K., and Johnston, J. P., "Near-Wall Structure of Three-Dimensional Turbulent Boundary Layers," *Proceedings of the 10th Symposium Turbulent Shear Flow*, Univ. of Pennsylvania, University Park, PA, 1995, pp. p-1-7–p-1-11.

[35]Baskaran, V., Smits, A. J., and Joubert, P. N., "A Turbulent Flow over a Curved Hill. Part 1. Growth of an Internal Boundary Layer," *Journal of Fluid Mechanics*, Vol. 182, Sept. 1987, pp. 47–83.

[36]Cantwell, B. J., "Organized Motion in Turbulent Flow," *Annual Review of Fluid Mechanics*, Vol. 13, 1981, pp. 457–515.

[37]Wu, X., and Squires, K. D., "Large Eddy Simulation of a Canonical Three-Dimensional Boundary Layer," *Proceedings of the 10th Symposium Turbulent Shear Flow*, Univ. of Pennsylvania, University Park, PA, 1995, pp. 1-8-19–1-8-24.